

© 2017 William Noll Kamerow

THE APPLICATION OF IMPREGNATING ARMATURE WINDINGS IN IRON RESIN
WITHIN HIGH-SPEED ELECTRIC MOTORS

BY

WILLIAM NOLL KAMEROW

THESIS

Submitted in partial fulfillment of the requirements
for the degree of Bachelor of Science in Electrical and Computer Engineering
in the Undergraduate College of the
University of Illinois at Urbana-Champaign, 2017

Urbana, Illinois

Adviser:

Professor Kiruba Haran

Abstract

This thesis summarizes the testing of an iron-filled resin to impregnate armature windings within a toothless air-core electric motor. The objective is to compare the magnetic permeabilities with thermal losses through an ecore test setup to extrapolate how the resin would behave within a high-speed electric motor. More specifically, the goal is to characterize the power losses within the iron resin using the Steinmetz equation to extrapolate the losses inside high speed electric motors. These characterizations were conducted using a calorimetric experiment to compute losses within the system. The results are important because by increasing the power output and maintaining a low weight, power density can be increased. The results of this experiment will help predict if an iron resin will increase the permeability allowing for a higher power density within the electric motors while keeping power emitted low. These experiments are run for the NASA Fixed Wing project to improve the power density of the electric motor to 8 HP/kg while maintaining 96% efficiency.

Keywords: Iron-filled resin, impregnate, Steinmetz, calorimetric, power density, electric motor, high-speed, high-frequency

To my parents, Harry and Sophia, for their love and support. I would like to thank individually my father for his unyielding push, guidance, and reassurance through my undergraduate career and my mother for her wisdom and inspiring advice to follow my passions, never settle, and always be happy. May she rest in peace.

Acknowledgments

I would like to acknowledge the entire Grainger Power Lab for teaching, assisting, and befriending me through the process of creating my thesis.

I would like to thank my advisor, Dr. Kiruba S. Haran, for advising and teaching me over the course of my senior thesis at the University of Illinois at Urbana-Champaign. His guidance and all encompassing mastery of the field helped immensely in understanding the experiments that led to writing my thesis.

Special thanks to Matt Feddersen for advising, teaching, befriending, and guiding me through the bumps in my thesis work. Without his support this thesis would have been much more difficult and a lot less fun. Thank you for your patience and effort in this endeavor.

Also I would like to thank Austin Jin for his help with creating the inductor, Lijun Zheng for helping me understand the thermodynamics as well as the in-depth photos of our motor, Nate Renner for his assistance in the creation of wire leads, Andy Yoon for his help with the Steinmetz analysis and curve fitting, and the Machine Shop at the University of Illinois at Urbana-Champaign for their mechanical advice.

Lastly, I would like to thank NASA and the Grainger Center for Electric Machinery and Electromechanics for their financial support of my research.

Table of Contents

Chapter 1	Literature Review	1
1.1	Background Information	1
1.2	Problem Motivation	2
1.3	Proposed Solution	4
Chapter 2	AC Losses with Resin and Litz Wire	6
2.1	AC Loss	6
2.2	Conductive Material Losses	7
2.3	Wire Losses	8
Chapter 3	Analytical Models	10
3.1	Saturation Values	10
Chapter 4	Calorimetric Loss Experiment	16
Chapter 5	Test Bench	19
5.1	Litz Wire Preparation	19
5.2	Sample Creation	19
Chapter 6	Results	27
6.1	Magnetic Field Results	27
6.2	Core and Wire Loss Characterization	29
6.3	Samples Losses	30
Chapter 7	Error Discussion	33
7.1	Sample Creation	33
7.2	Magnetic Field Simulation	33
7.3	Air Loss Equation and Experimental Data	34
Chapter 8	Conclusion	35
8.1	Future Work	35
Chapter 9	References	37
Appendix A	Appendix	38
A.1	Matlab Code	38
A.2	Samples	48

Chapter 1

Literature Review

1.1 Background Information

The prevalence of electric motors is growing exponentially every year within the transportation industry due to safety, lower noise pollution, and energy efficiency [1]. According to the International Air Transport Agency (IATA), in 2010 2.4 billion passengers and 40 million tons of goods were transported via the skies based on data collected over the past 40 years [2]. To meet this demand for airspace utilization and higher aircraft energy efficiency, electric machines with extremely high power densities are now being considered.

High-power dense electric motors for aerospace applications are being developed for the NASA Fixed Wing Project to create an air-core, high-frequency motor [3]. The general design of the machine is illustrated in Figure 1.1, with the rotor unconventionally placed on the outside of the machine. This motor is a high-speed permanent magnet synchronous machine with a slotless stator.



Figure 1.1: Diagram of Air-Core, High-Frequency Motor

The particular assembly of the windings of the motor allows free space in between the copper windings and stator. By creating a low reluctance path using an iron resin, the

flux flowing is increased by effectively shortening the airgap. Determining the different composites to create a more permeable path for the flux within the motor to travel through is discussed more thoroughly in [1]. Once the correct composite is chosen, understanding the power loss in the composite is the next step in using this resin within a high-speed electric motor.

The iron-filled resin will increase the permeability of free space between the copper wires and stator, but at high frequencies there is a risk of the resin generating heat through various loss mechanisms. This thesis will discuss the testing of different combinations of wire and resin to characterize the losses that occur within the resin inside high-speed electric motors.

1.2 Problem Motivation

The power density is the value that is important for electric motors in the transportation industry because the less weight a vehicle or plane has to transfer, the more efficient it becomes. The power density of an electric motor is governed by the equation below:

$$P_D = \frac{P_m}{W} \quad (1.1)$$

where P_D is the power density, P_m is the total power output, and W is the weight of the motor. Power output in a three-phase electric motor is proportional to the phase current I_ϕ and phase voltage E_ϕ . Equation 1.2 indicates that by increasing the armature current within the armature windings of an electric motor the power output will increase. However, current is directly related to temperature by DC and AC losses. The amount of heat the material can sustain is the threshold for how much current the motor can withstand. Therefore, the insulation and temperature ratings of the material in combination with the cooling method define the maximum current allowed to flow through the armature windings [2]. Currently, superconductors are being researched to increase the current flow while keeping the power loss low [4].

$$P_{output} = 3E_\phi I_\phi \quad (1.2)$$

In this equation P_{output} is the power output by the motor. This current is proportional to the flux produced in the electric motor by Ampere's law. The iron teeth of the electric motor are wrapped in wire called armature windings. When current runs through the armature windings a magnetic field is created because of Ampere's law. This magnetic field induces an opposing magnetic field in the rotor. The induced magnetic field then creates a torque on the rotor, causing the rotor to rotate.

While iron teeth are used in most motors, the NASA fixed motor is of the slotless configuration. Slotless electric motors have armature windings that are not wrapped around iron teeth and generate flux through the airgap of the motor. A common problem with this design is that during operation the windings will move or shake due to instability. The instability is because the motor lacks iron teeth to hold the armature windings. Yet these motors are ideal for maximizing power density because having no iron teeth reduces the weight of the motor. One solution to solve the instability of armature windings as well as increase power output is impregnating the armature windings in an iron resin.

Currently, the state of the art for motors using this technology is axial flux machines and slotless electric motors. By not having iron teeth, we reduce eddy losses and the weight of the motor [1]. Nonetheless, by not having iron teeth the motor now has free space in between the armature windings. To enhance this type of motor, inserting a material in between the stator windings could possibly create a higher effective permeability path for the flux to flow. A higher flux flow will increase the power output while keeping the weight low. In Figure 1.2 there is a slotted electric motor to the left and a slotless electric motor to the right. The slotted motor has bars within the labeled lamination shoes attached in the left image. Around the lamination shoes, the armature wires are wrapped around iron teeth. The slotless electric motor design on the right-hand side does not have lamination shoes where the iron teeth would be. This figure shows free space in between the armature windings.

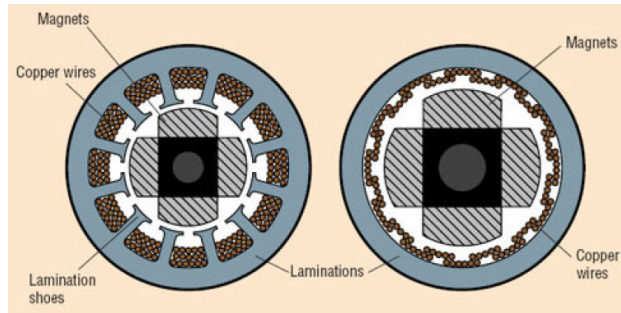


Figure 1.2: Slot and Slotless Electric Motor [1]

1.3 Proposed Solution

One method to increase the flux within an armature winding is to increase the flux through the armature coils via an iron resin. Figure 1.3 is a zoomed-in picture of the Nasa Fixed Wing motor slotless region. In this diagram the half black circle within the two red regions is an example of an armature winding. The space enclosed by the armature winding is where the resin would exist. Current is run through the windings of the stator. This current creates a magnetic field with which the magnets on the rotor will try to align, causing the rotor to rotate. In between the armature windings and stator is a body of free space. The magnetic permeability of this free space is given to be $4\pi * 10^{-7}$. Improving the permeability with a material that has a higher magnetic permeability than air would enable the motor to transfer more flux through the armature windings [1]. The winding would be impregnated with this iron resin, thereby increasing the magnetic permeability.

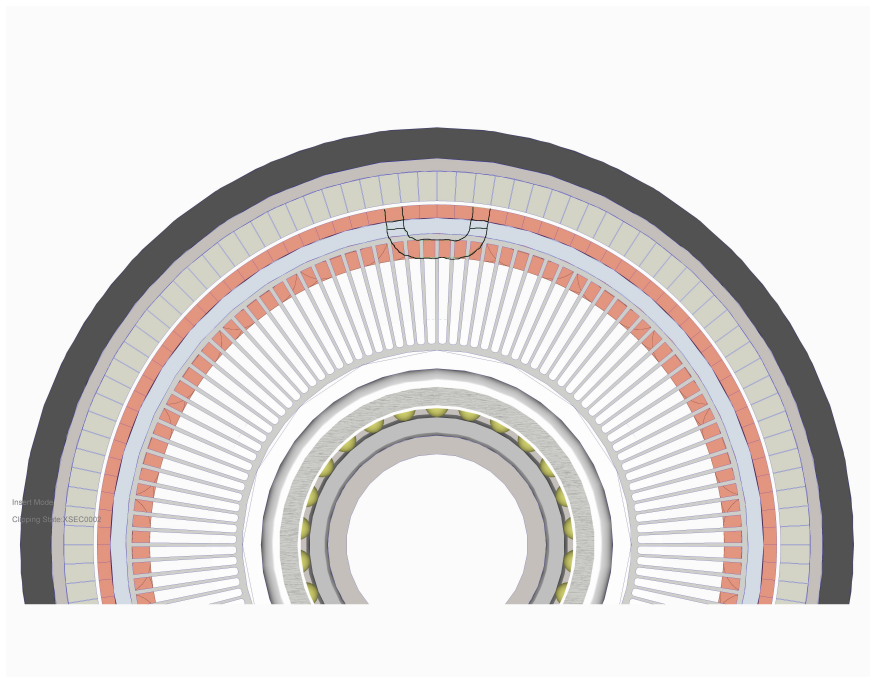


Figure 1.3: Toothless Electric Motor Sketch

Chapter 2

AC Losses with Resin and Litz Wire

This chapter will go over AC losses that occur due to electromagnetic effects in this experiment. The type of wire used in this experiment is Litz wire because Litz wire nullifies the proximity and skin effects. Proximity and skin effect will be briefly discussed as this is a well covered topic in the literature.

2.1 AC Loss

AC loss occurs within electric motors due to a changing armature phase current. AC losses are mainly dependent on the frequency of the signal, and they are important in high-frequency electric motors because they are proportional to frequency. In this experiment, different types of losses contribute to the rise in temperature of the system. The Litz wire losses come from the skin effect and proximity effect and the core losses come from eddy current and hysteresis losses.

Unlike their DC counterparts, which have losses equal to I^2R , AC losses transpire when an alternating current is running through a conductor. A changing voltage within a conductor causes charged particles inside the conductor to move back and forth very quickly. Charges moving back and forth, creating a time-varying current which in turn creates a changing magnetic field (\mathbf{B}) because of Faraday's law shown in Equation 2.1. This equation indicates that a non-conservative electric field (\mathbf{E}) within the conductor will be produced at the same frequency of the changing voltage generated initially. Therefore a non-uniform field will exist inside the iron resin from an AC source. This non-uniform field exists specifically in the slotless area of electric motors. These nonuniformities go on to create eddy currents.

Eddy currents are a form of loss and are discussed in [2].

$$\nabla \times E = -\frac{dB}{dt} \quad (2.1)$$

2.2 Conductive Material Losses

Conductive material losses are losses in the iron resin and ecore material that materialize because of an alternating flux. These losses are also known as iron losses [5].

2.2.1 Eddy Current Losses

Eddy currents arise in a changing magnetic field inside a conductive material. This experiment's conductive materials are both the iron resin and the ecore material. Eddy currents are small circular currents that flow within these types of materials. Eddy currents circulate to generate a magnetic field of their own to oppose the created magnetic field induced on them by a source due to Lenz's law, [6] which any current induced within a wire from another magnetic field will establish an opposing magnetic field by inducing another current inside its own system. These other currents induced in the system are called eddy currents. However, the experiment uses Litz wire that mitigates eddy currents within itself, but not the surrounding resin [2].

Illustrated Figure 2.1 is a magnet that generates a magnetic field in one direction. The conductive material below creates an opposing magnetic field by inducing a current within its self. These currents are one form of loss within the resin.

2.2.2 Hysteresis Losses

The other type of loss that occurs within the iron resin and ecore is hysteresis. Hysteresis occurs from a conductive material becoming magnetized from a magnetic field. Once the magnetic field changes direction, as in an AC source, the material that was previously magnetized in one polarity must be magnetized in the opposite direction. The changing

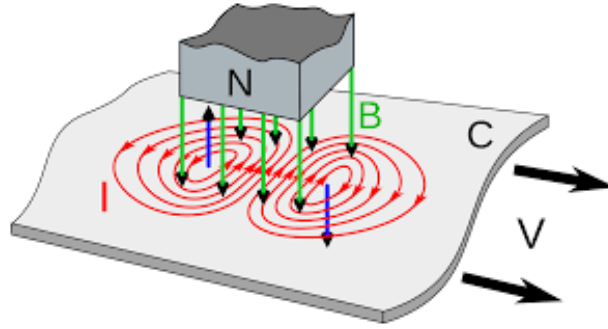


Figure 2.1: Eddy Current Example [7]

polarity of the magnetic particles inside the conductor is what causes hysteresis. A common way to analyze hysteresis losses is to generate a B-H loop that indicates the amount of power put into the system to change the magnetic field direction. In order to best understand this error, running the material at saturation (0.4 Tesla) will give the best results. This information is taken from the resin 117 Cuming datasheet for the iron resin.

2.2.3 Magnetostriction

The last type of loss is magnetostriction, which occurs when ferromagnetic materials get magnetized. When the material becomes magnetized it changes its shape. In this experiment the ferromagnetic materials changed their shape slightly during the process of testing because the conductive materials kept rapidly constricting and expanding, producing a high-pitched noise. Characterizing this type of loss is beyond the scope of this thesis.

2.3 Wire Losses

This section will discuss losses within the Litz wire. The first type of loss is the skin effect loss. The second type is the proximity effect loss discussed in more depth in [2].

2.3.1 Skin Effect and Proximity Effect

Equation 2.2 describes skin effect resistance where \mathfrak{R} is the resistance, ρ is the resistivity, l is the length of wire, and A is the effective conduction area. In [2] the explanation of skin effect blocking out magnetic fields is described.

$$\mathfrak{R} = \frac{\rho l}{A} \quad (2.2)$$

The proximity effect occurs when multiple strands of wire induce a magnetic field on each other because they are conducting current. This causes the current to group into small regions of the wire, there by increasing the resistance of the wire. Increasing the resistance increases the power loss in the wire. To reduce the effects of both skin and proximity effect, Litz wire is used. Since these losses are nullified in this experiment, this thesis will not cover this topic. The proximity effect is discussed in detail in [2].

Chapter 3

Analytical Models

In this chapter we will try to predict the current and voltage needed to bring our experiment to saturation. Saturation allows hysteresis and eddy losses to be observed better within the experiment. The Cumin data sheet indicates that 0.4 Tesla is needed to saturate the resin. The ecores saturate at 0.5 Tesla. The Steinmetz method separates losses into individual eddy and hysteresis losses within the resin samples. The models are MATLAB and Flux based.

3.1 Saturation Values

knowing that the resin saturates at 0.4 Tesla enables solving the current and voltage by the magnetic circuit, which in turn enables calculating the reluctance (\mathfrak{R}). In [1], the author uses the same ecore design as the experiment's test setup. The calculations in [1] are used to find the dimensions of the ecore.

3.1.1 Magnetic Circuit

The approximate ecore design and

dimensions are shown in Figures 3.1 and 3.2 respectively, which enable the solution circuit in Figure 3.3,

where \mathfrak{R}_g is the reluctance of the gap, \mathfrak{R}_2 is the reluctance of the two legs of the ecore combined and \mathfrak{R}_1 is the reluctance of the top branches of the ecore divided by two.

$$\mathfrak{R} = \frac{l}{\mu_0 A} \quad (3.1)$$

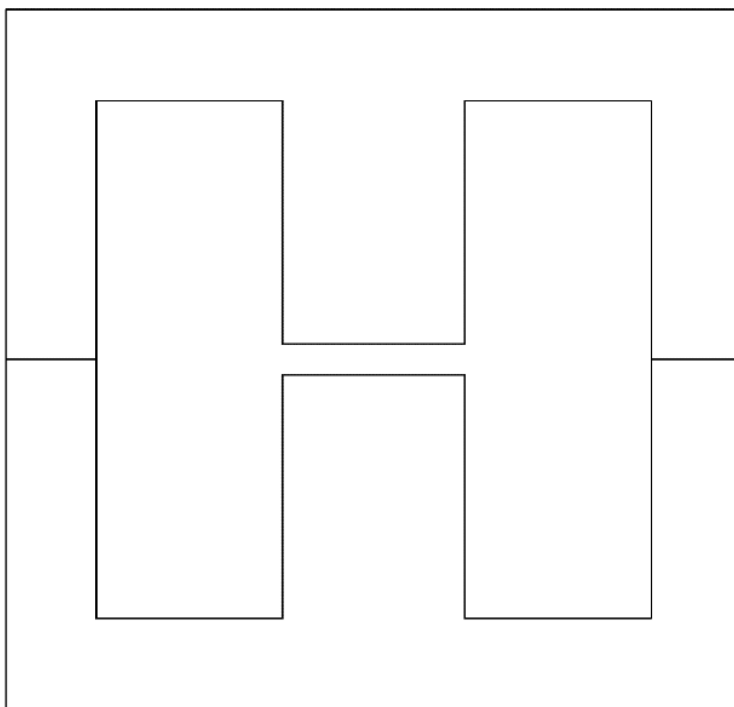


Figure 3.1: Ecore Design

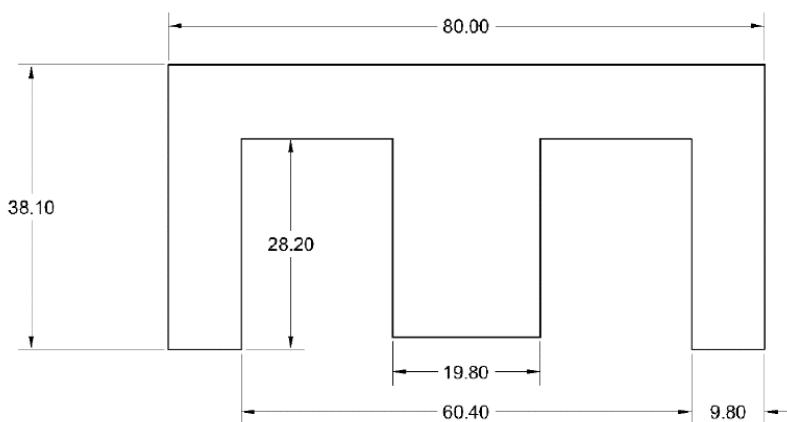


Figure 3.2: Ecore Dimensions

Each reluctance for the magnetic circuit is calculated by Equation 3.1 where the reluctance is R , l is the length of the region, and A is the cross-sectional area.

With all reluctances solved, the total reluctance of the circuit can be calculated. The sample in the gap between the ecores determines the reluctance for each experiment. Therefore, each experiment will have a different maximum current and voltage saturation value.

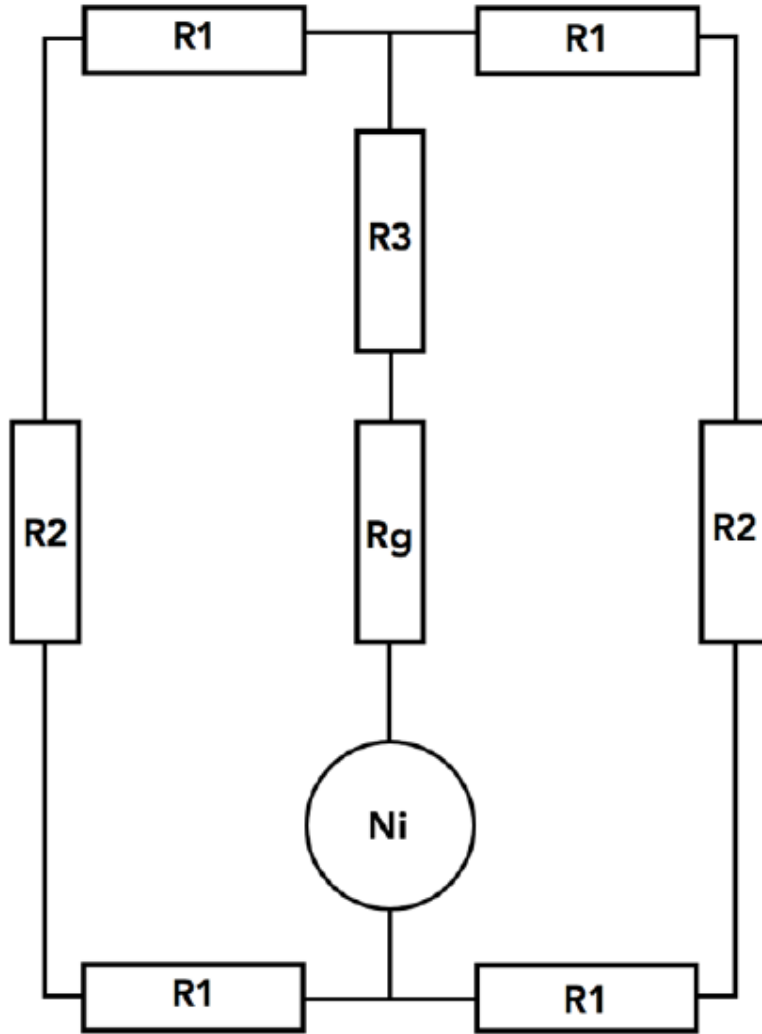


Figure 3.3: Magnetic Circuit

3.1.2 Magnetic Equations

The reluctance is related to flux by Equation 3.3. The total flux can be calculated by using Equation 3.2.

$$\phi = B_{iron}A_{gap} \quad (3.2)$$

where ϕ is the max flux, B_{iron} is the saturation value from the resin data sheet, and A_{gap} is the smallest cross-sectional area in the ecore. With the max flux solved the current relation can be solved for.

$$I_{max} = \frac{\phi \mathfrak{R}}{N} \quad (3.3)$$

where I_{max} is current, ϕ is total flux, \mathfrak{R} is reluctance, and N is the number of turns in the excitation coil. The inductance is related to the reluctance by Equation 3.4.

$$L = \frac{N^2}{\mathfrak{R}} \quad (3.4)$$

where L is the inductance, N is the number of turns in the excitation coil, and \mathfrak{R} is the reluctance of the magnetic circuit. Then the voltage can be solved for with the inductance from Equation 3.4. Equation 3.5 is solved by the equation relating voltage to an inductor.

$$V = L \frac{dI}{dT} = L \frac{\Delta I}{\Delta T} = L \frac{2I_{max}}{\frac{T}{2}} \quad (3.5)$$

The equation describing the current in the inductor is described by a triangular wave. The maximum current (I) would occur at a change in current divided by two. The time of maximum change is equal to one half the period (T). By resolving Equation 3.5 for voltage, Equation 3.6 is found.

$$V = 4LI f \quad (3.6)$$

where V is the voltage, L is the inductance, I is the current, and f is the input frequency from the source.

3.1.3 Matlab Code and Finite Element Model

The experiment's Matlab models are based on the magnetic equations derived above. The Matlab code solved for the different saturation voltage and current values. Attached in the appendix is the Matlab code written for this experiment. The voltage, current, and power test plots showed trends where the voltage applied is independent of the gap length and type of sample. The current plot shows that when gap length is increased, current supplied needs to be increased. Also the plots indicate that the resin needs less current to saturate than air.

With an increase in the gap length, our required current and power increase linearly. However, the required voltage does not change. This makes sense because an increase in gap

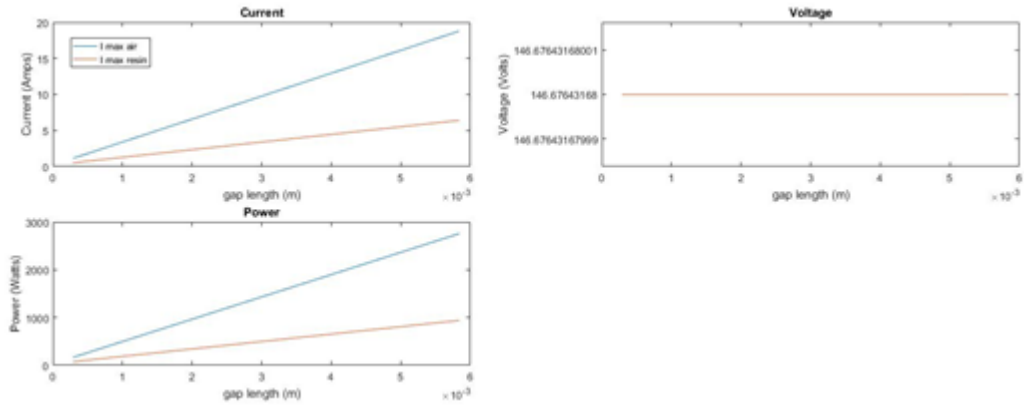


Figure 3.4: Voltage, Current, and Power Test Plots

length would increase the current and decrease the inductance.

Once the voltage, current and power were calculated, a finite element model was created in Ansys Maxwell to compare the Matlab results.

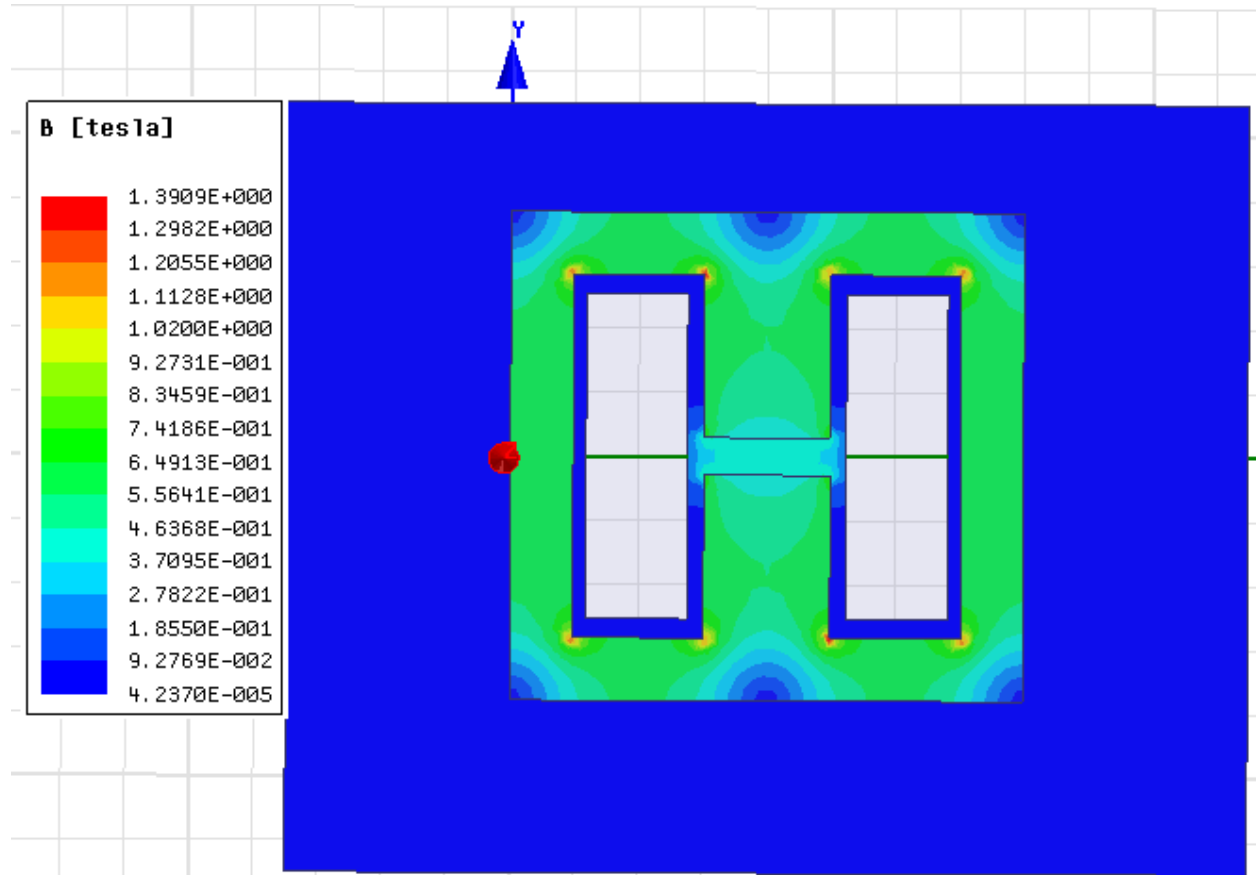


Figure 3.5: Finite Element Model of Resin Test

The model indicates that the magnetic field strength in the ecore is 0.4 Tesla, indicating that our MATLAB code was successful in predicting the expected B field.

Chapter 4

Calorimetric Loss Experiment

This chapter will discuss how to convert a change in temperature to a power loss equivalent by using a calorimeter. The previous chapter confirmed that our Matlab code to predict saturation current and voltage values was correct to get the predicted magnetic field. With the current and voltage predicted for saturation, all that was left was to convert AC losses in the form of heat to a power loss.

In order to determine the power loss from the experimental setup, a standard on how to convert temperature to power was needed. To do this, a constant metal bar resistor of 264Ω was placed into the test setup with a 12 V supply. The metal bar acted as constant power going into the system. When the heat leaving the calorimeter equals the heat entering the system, the system's temperature stops changing, indicating a certain power input equals a certain temperature change observed. In Figure 4.1 is an sample of data from a constant DC input of 41 V.

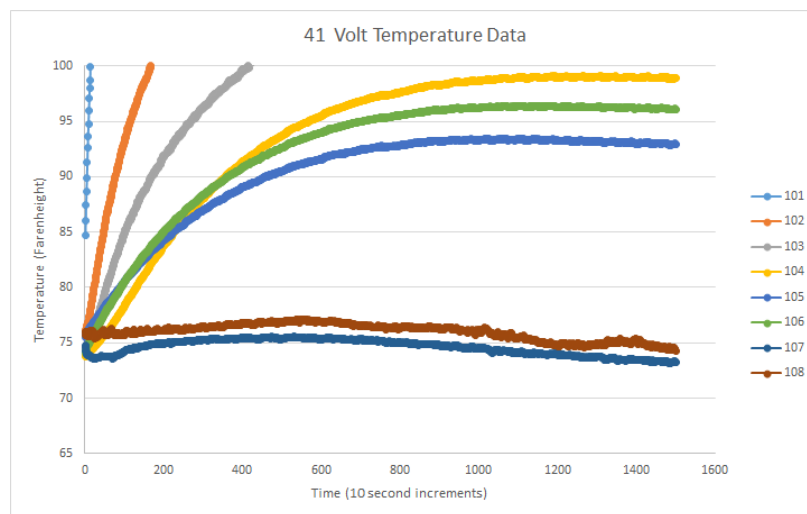


Figure 4.1: 41 V Temperature Calibration Data

In Figure 4.1 the different lines represent different temperature readings from each thermocouple. The type of thermocouples used were J and K type. The J and K type thermocouples have maximum and minimum operation temperatures that exceed the maximum and minimum of this experiment. Thermocouples 105 and 106 are inside the calorimeter setup on opposite walls of the calorimeter. Thermocouple 107 and 108 are attached to the outer walls of the calorimeter. These thermocouples represent the ambient temperature in the room. The other thermocouples were used to monitor different points within the experiment to monitor the temperature to avoid overheating the system.

The goal is to create a standard plot for this experiment representing the temperature change with an input power. To obtain the temperature change the last 100 points of 105 and 106 are averaged. Then the last 100 points of thermocouple 107 and 108 are averaged to give the outside ambient temperature. Then the difference of the two averages indicates the change in temperature at saturation for our calibration curve. In Table 4.1 is the experimental data for the thermocouples. In Figures 5.12 and 5.13 on page 24 and 25 are the calibration test setup.

Table 4.1: Calibration Table

$P(W)$	$\delta T(C^\circ)$
0.54	2.52
1.826	4.12
2.754	5.56
4.655	8.95
6.355	1.42
7.348	12.87
9.45	15.67

In Figure 4.2 the change in power vs temperature is plotted. Thereupon a linear line is fitted to the calibration data set and its slope is 0.6572. The value is called the calibration coefficient σ [W/°C] and is unique to this experimental setup.

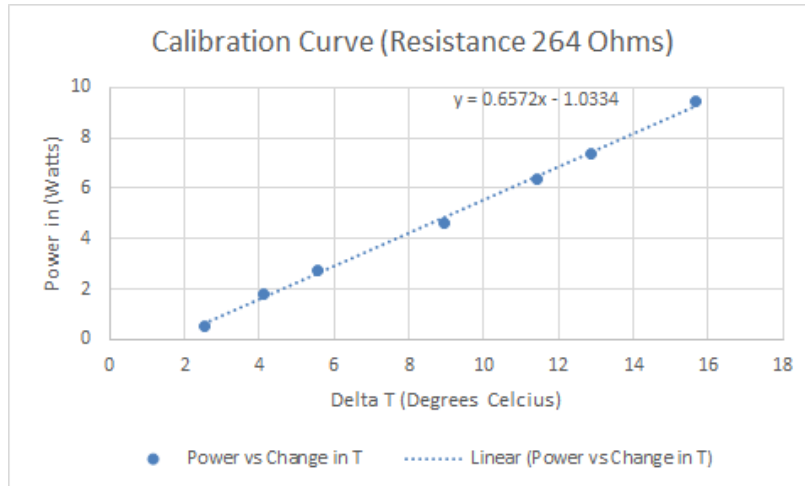


Figure 4.2: Calibration Curve

$$P_{input} = .6572\Delta T^{\circ}C \quad (4.1)$$

Chapter 5

Test Bench

This chapter will discuss all methods to collect the experimental data.

5.1 Litz Wire Preparation

The first step of the experiment is to prepare the Litz wire. An example of Litz wire is shown in Figure 5.1 . The amount of wire cut is the amount to wrap around the radius of the bobbin to the inner side of the ecore. RTV is applied to the Litz wire to provide extra support to the wire so the wire would not come undone during the winding process. RTV is room temperature vulcanization silicone. Figure 5.2 is the finished wound bobbin inductor. Once the inductor was wound around the bobbin a strong base removed the insulation from the lead ends. Lastly a lug nut connected the 120-ASX Pacific Power source to the inductor. The maximum frequency of the source is 1200 Hz with a maximum voltage of $150 V_{line-line}$. The source is presented in Figure 5.3.

5.2 Sample Creation

3D printed polycarbonate casts were created to create a mold for the iron resin samples. In Figures 5.1, 5.4 and 5.6 are the casts created in Solidworks. Subsequently, the PDMS molds created from the casts were filled with iron resin. PDMS stands for Polydimethylsiloxane and is a type of silicon. The resin then was cured within the PDMS molds and then taken out of the molds to be cut to size for experimentation.

There are indentations in Figure 5.4 and 5.5 for the wire to sit within the resin and be pressed down during the curing process. This is done because the sample needs to have the



Figure 5.1: Litz Wire

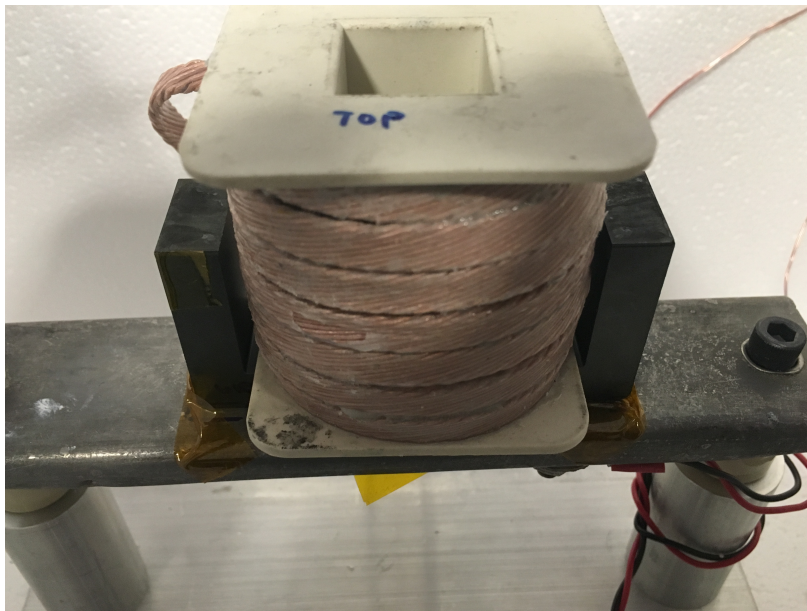


Figure 5.2: Wound Inductor Setup

wires be uniform throughout.



Figure 5.3: 120-ASX AC Source

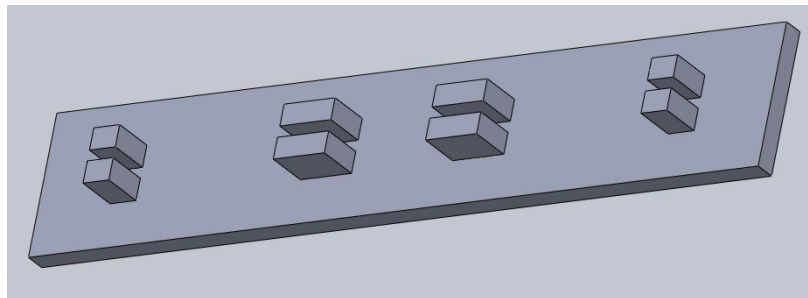


Figure 5.4: Top Cast 1

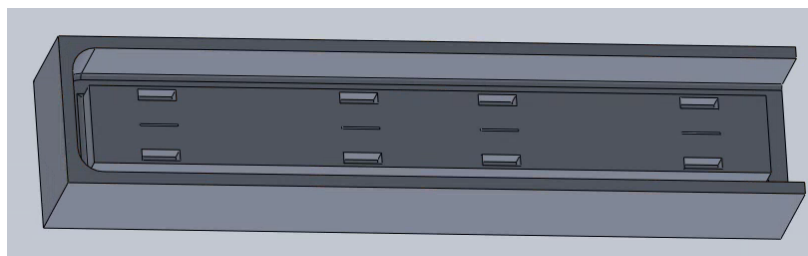


Figure 5.5: Bottom Cast 1

5.2.1 PDMS

Using the casts, PDMS molds are created. The curing for the mold was done in Talbot labs on the University of Illinois campus. A more detailed report of the curing process is described in [1].

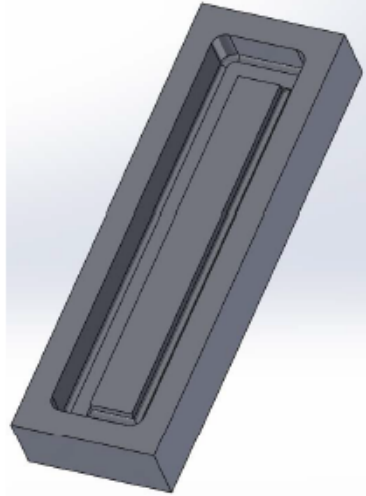


Figure 5.6: Bottom Cast 2



Figure 5.7: Polycarbonate Cast



Figure 5.8: PDMS Mold for Resin

5.2.2 Samples

The samples are cut to the size of the cross section of the ecore which is a 20 mm x 20 mm square. The gap between the ecores is 4 mm. In Figure 5.11 are the samples prepared for the experiment.

In Figures A.1, A.2, A.3 are the three samples individually.

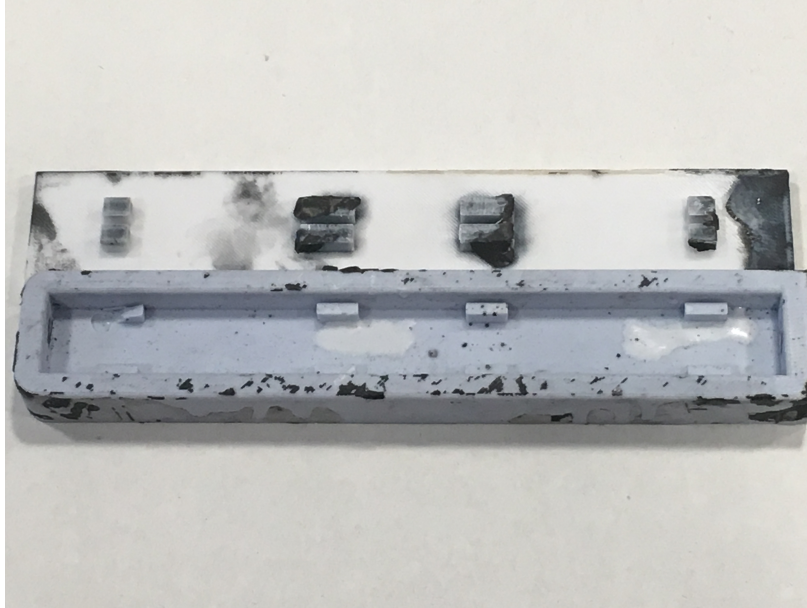


Figure 5.9: PDMS Mold for Wires in Resin and Cap

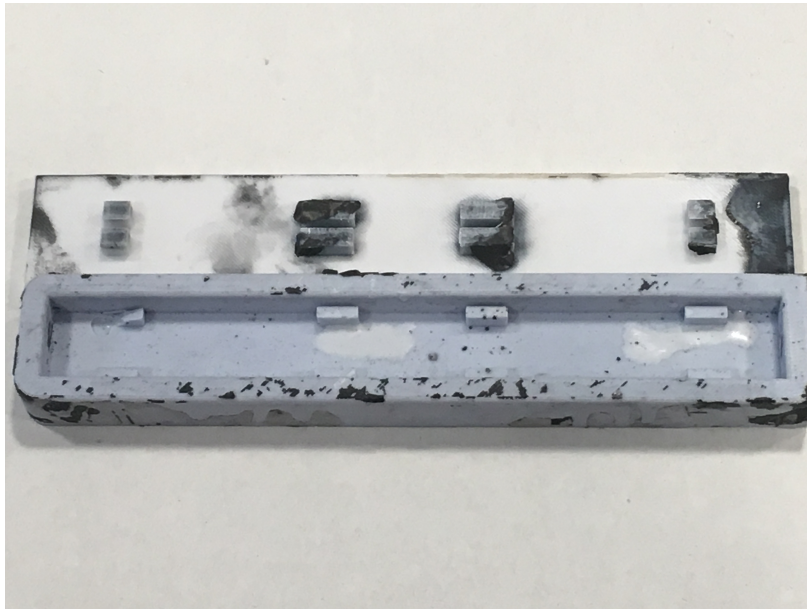


Figure 5.10: PDMS Mold for Wires in Resin

5.2.3 Test Bench

With all materials gathered, testing could begin. In Figure 5.12 is the experimental test-bench. The system was enclosed by a styrofoam box as shown in Figure 5.13.

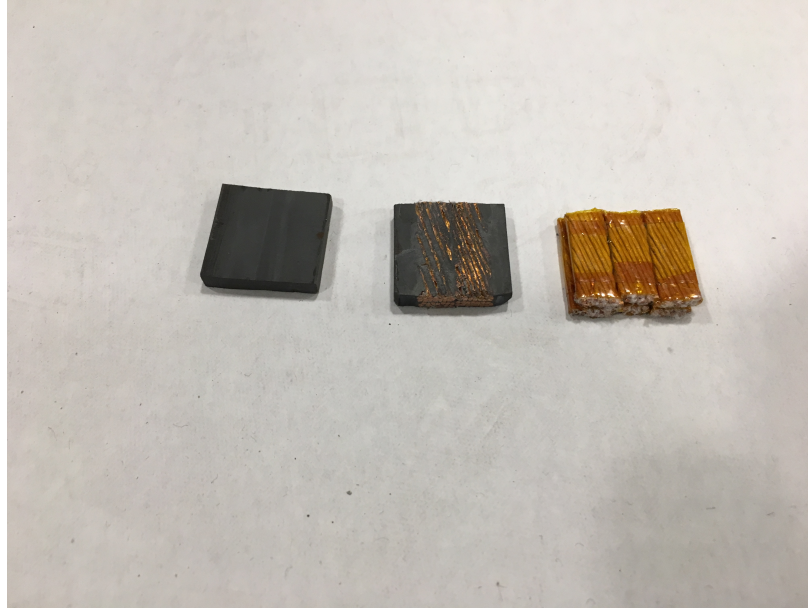


Figure 5.11: Left Resin sample. Middle Wire Resin Sample. Right Wire Sample.

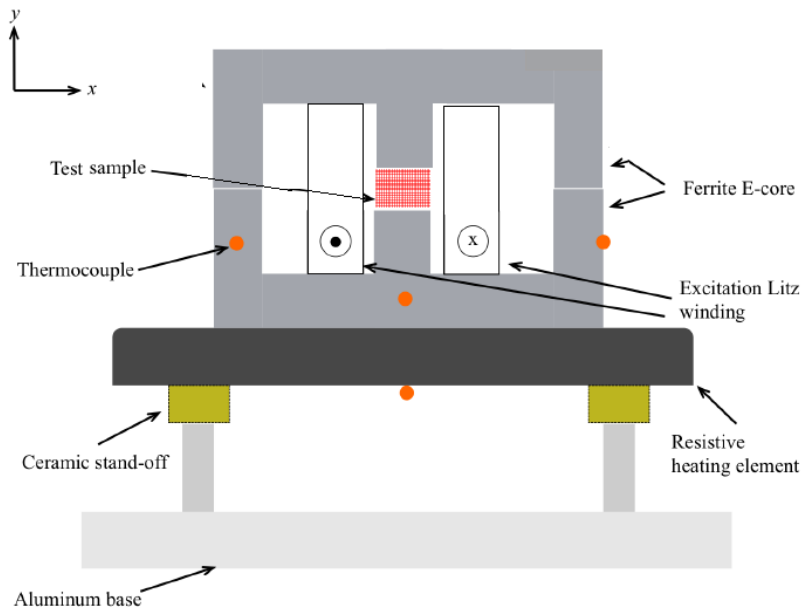


Figure 5.12: Testbench Model

5.2.4 Pickup Coil

After the temperature data was collected, a pickup coil was created to measure the magnetic field in each case. The experimental magnetic field value is measured to compare with the theoretical results from the Matlab code. Attached in the appendix under *Experimental_B*

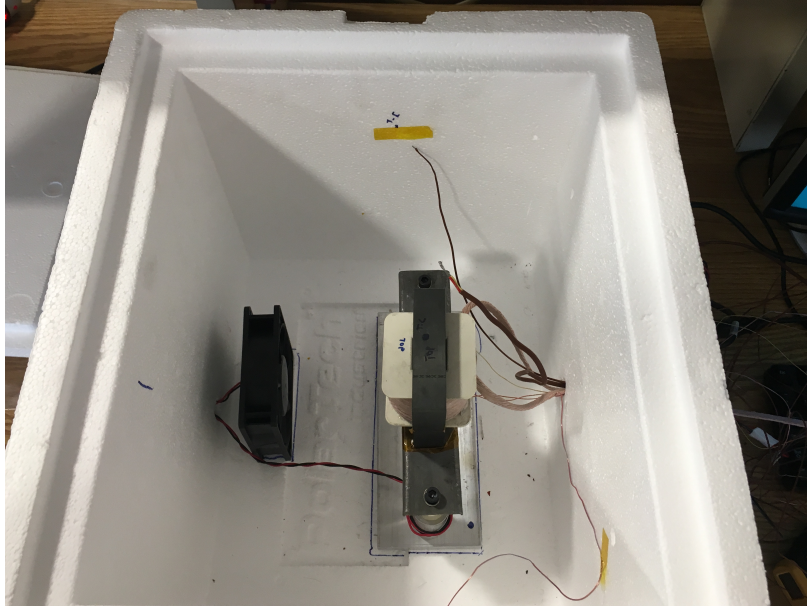


Figure 5.13: Experimental Testbench

is the code to convert the induced voltage in the coil to a respective B field in the core. Figure 5.14 shows the pickup coil designed to solve for the magnetic field in the coil. The pickup coil has an induced voltage because the ecore has a changing magnetic field running through it due the AC current running through the inductor. The pickup coil had 16 turns around the ecore.

$$\lambda = NBA = \int_a^b v(t)dt \quad (5.1)$$

where λ is the flux linkage, N is the number of turns around the ecore, B is the rms magnetic field, A is cross sectional area of the small leg of the ecore, and $\mathbf{v}(\mathbf{t})$ is the induced EMF in the pickup coil.

$$V_{rms}\sqrt{2}\sin(\omega t) = v(t) \quad (5.2)$$

where V_{rms} is the voltage read from the multimeter across the pick up coil and ω is the frequency in rad/s. Lastly solving for the peak magnetic field (B) the equations above can be simplified to Equation 5.3

$$B_{peak} = \frac{V_{rms}\sqrt{2}}{\omega NA} \quad (5.3)$$

5.2.5 Airgap

One way to change the magnetic field is to change the reluctance by increasing the airgap in between the ecores. The chosen airgap for experimentation was 1 mm. In Figure 5.15 is the 1 mm spacer attached to the ecore.

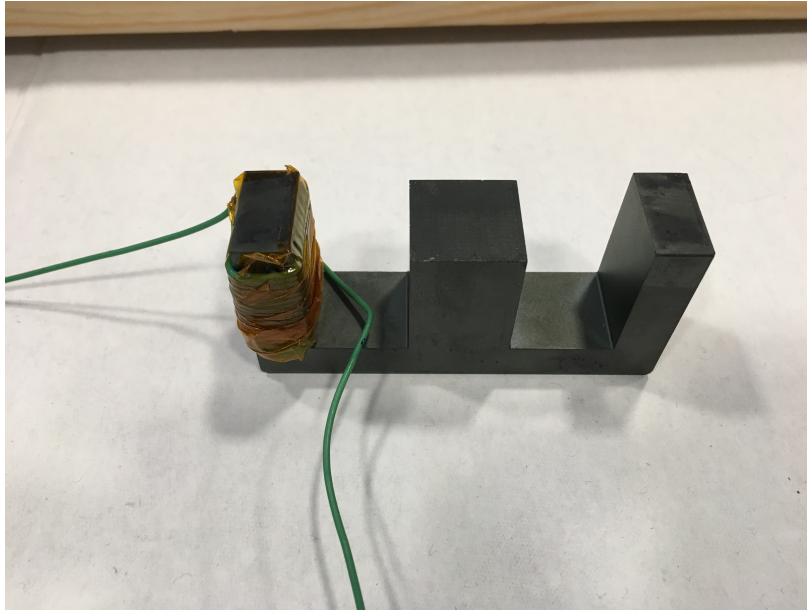


Figure 5.14: Pickup Coil

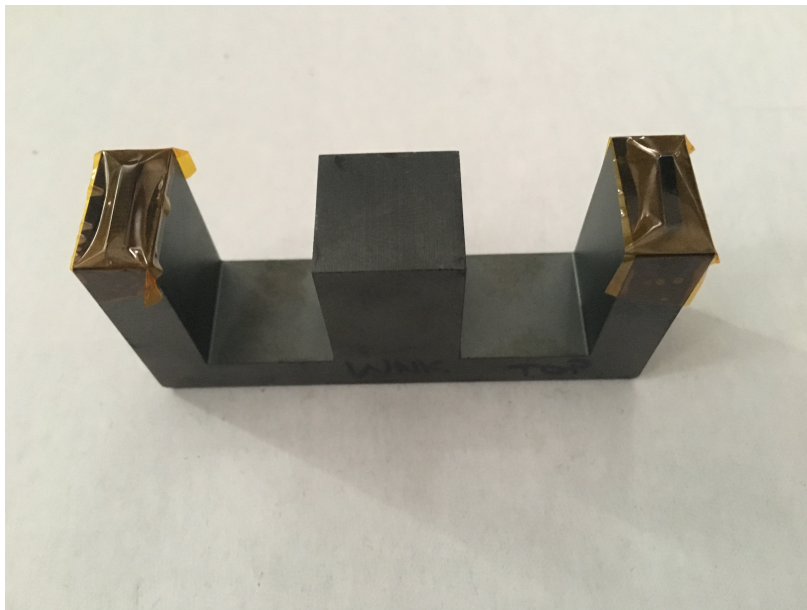


Figure 5.15: Ecore with 1 mm Spacer Attached

Chapter 6

Results

This chapter contains all data collected and analyzed.

6.1 Magnetic Field Results

The first step to analyzing the data is to compare the experimental magnetic field with the theoretical data models. The experimental magnetic field is calculated from the induced voltage in the pickup coil. Equations 5.1-5.3 show how to solve for the experimental B field. In Table 6.1 the experimental magnetic field is compared to the theoretical magnetic field generated by our models. The model's equations can be reversed to calculate for the magnetic field in the process below. Attached in the appendix under Reverse B is the Matlab code to solve for the **B** field.

$$\phi = \frac{NI_{rms}\sqrt{2}}{R_{total}} = BA \quad (6.1)$$

$$\frac{NI_{rms}\sqrt{2}}{R_{total}A} = B \quad (6.2)$$

where ϕ is the flux in the leg of the ecore, B is the magnetic field in the sample, A is cross sectional area of the middle region, N is the number of turns in the inductor, I_{rms} is the current applied by the AC source and R_{total} is the total reluctance of the ecores and airgap added together.

The percent error between the experimental and theoretical magnetic fields is calculated with the equation below.

$$Error\% = \frac{B_{experimental} - B_{theoretical}}{B_{theoretical}} * 100\% \quad (6.3)$$

In Table 6.1, ‘117’ indicates a pure iron resin sample, ‘117W’ indicates a wire sample covered with resin, ‘Wire’ indicates a wire sample, and ‘Air’ indicates an air sample. Lastly, ‘1 mm gap’ represents the addition of the 1 mm plastic piece between the ecore pieces.

Table 6.1: Magnetic Table

Sample	1mm Gap	$f(Hz)$	$I(A)$	$V_{induced}$	$B_{theo}(T)$	$B_{exp}(T)$	Error %
117	No	60	15	0.41	.952	.4924	48.3
117	No	600	15	4.11	.952	.4912	48.4
117	No	1200	15	8.19	.952	.4918	48.4
117W	No	60	15	0.414	.580	.4972	14.3
117W	No	600	15	0.494	.580	.4936	15.1
117W	No	1200	15	0.492	.580	.4924	15.1
Wire	No	60	15	0.332	.328	.3315	1.12
Wire	No	600	15	0.323	.328	.3279	.026
Wire	No	1200	15	0.327	.328	.3273	.157
Air	No	60	15	0.405	.328	.4864	48.4
Air	No	600	15	4.030	.328	.4840	47.6
Air	No	1200	15	8.070	.328	.4864	47.8
Air	No	60	10	0.270	.219	.3206	46.7
Air	No	600	10	2.580	.219	.3098	41.8
Air	No	1200	10	5.160	.219	.3098	41.8
Air	Yes	60	15	.2680	.239	.3218	34.4
Air	Yes	600	15	2.610	.239	.3134	30.9
Air	Yes	1200	15	5.240	.239	.3146	31.4
Air	Yes	60	10	.1780	.159	.2138	33.9
Air	Yes	600	10	1.770	.159	.2126	33.2
Air	Yes	1200	10	3.500	.159	.2102	31.7

The 117 and 117Wire sample have similar magnetic field results because the ecore saturates at 0.5 Tesla. This was discovered after the test taking process, meaning more data will need to be taken. The experiment needs to be designed so the B field is limited to 0.5 Tesla because the ecore saturates at that point. Also the theoretical air samples B field differ by a factor of $\sqrt{2}$ from the experimental data. This indicates that there may be an error within the model.

6.2 Core and Wire Loss Characterization

The experimental magnetic field data is used for the the air loss calculation. The next step is to solve an equation describing losses within the air. This loss equation is a baseline equation to compare with the resin and wire sample losses. An equation relating current, magnetic field, and frequency was generated for air samples in order to compare the resin and wire power losses. In Table 6.2 the air loss data is presented. In the air core sample the losses are wire losses, hysteresis, and eddy losses in the ecores. Wire losses are proportional to I^2R . Hysteresis losses are proportional to the frequency (f) times the magnetic field squared (B^2). Eddy current losses are proportional to frequency squared (f^2) times the magnetic field squared (B^2). Adding all these losses together allows for the derivation of the equation below.

$$P_{loss} = k_1 I^2 + k_2 B^2 f^2 + k_3 B^2 f \quad (6.4)$$

This equation's coefficients are solved by taking experimental data and fitting it to Equation 6.4 using the MATLAB curve fitting tool. The data acquired is in table 6.2.

Table 6.2: Air Loss

$f(Hz)$	Air Gap	$B(T)$	$I(A)$	$P_{exp}(W)$
60	No	.4864	15	6.00391
600	No	.484	15	6.76704
1200	No	.4846	15	9.03095
60	No	.3206	10	2.38378
600	No	.3098	10	2.86248
1200	No	.3098	10	3.42636
60	Yes	.3218	15	6.37887
600	Yes	.3134	15	7.98908
1200	Yes	.3146	15	9.42101
60	Yes	.2138	10	2.54
600	Yes	.2126	10	3.0052
1200	Yes	.2102	10	3.58606

The data shows higher losses for a larger airgap, which contradicts expected results from

the theory. This is because the reluctance has increased in the system causing less flux to flow, meaning less AC loss. In figure 6.1 is the output from the Matlab curve fit tool. The x axis is the frequency (Hz), y axis is $\frac{P}{B^2}$ and the z axis is $\frac{I^2}{B^2}$. The variables were chosen this way in order to make the Matlab curve fitting tool operate correctly. The Matlab curve fitting tool only accepts two variables therefore by dividing by B^2 everywhere the curve fitting tool can process the data.

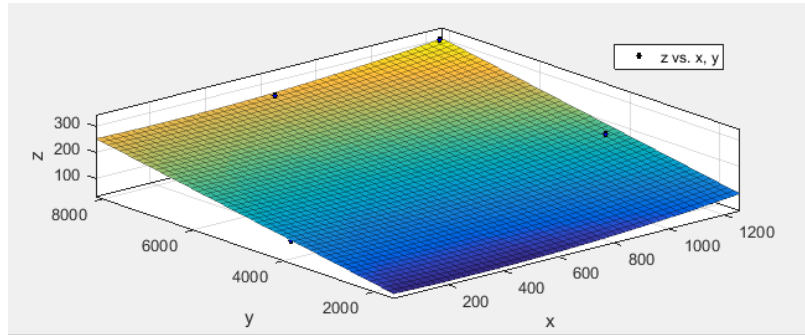


Figure 6.1: Air Loss Curve Surface

The curve matched the data to the equation below with an R^2 value of 92%. The R^2 value indicates how close each point is to the fitted curve. The closer the value is to 100% the better the curve matches the data. The coefficient's magnitude indicates the conduction loss and eddy current losses make up the majority of the air sample loss in the experiment. The hysteresis losses are small in comparison.

$$P_{loss} = .02942I^2 + 1.263 * 10^{-5} B^2 f^2 - .002727B^2 f \quad (6.5)$$

This equation can be used as a baseline for core losses and winding losses during the calorimetric experiment.

6.3 Samples Losses

With the equation derived for the core and wire losses in a pure air sample solving for the losses that only occur in resin is rudimentary. Subtracting the air samples power losses from the power losses of the sample gives the hysteresis and eddy current losses in the sample

piece. This is the goal to characterize losses of a high speed electric motor if impregnated armature wires were used with resin. In Table 6.3 the rest of our experimental data is presented. P_{loss} in equation 6.5 is equal to P_{air} . P_{sample} is equal to $P_{exp} - P_{air}$ because P_{air} takes into account all losses except the sample losses.

Table 6.3: Air Loss

Sample	$f(Hz)$	$B(Teslas)$	$I(Amps)$	$P_{exp}(W)$	P_{air}	$P_{sample}(W)$
117	60	.4924	15	6.29313	6.5931	-.299
117	600	.4912	15	10.6385	7.3224	3.314
117	1200	.4918	15	14.0238	10.229	3.794
117WIRE	60	.4972	15	6.2911	6.59	-.301
117WIRE	600	.4936	15	9.603	7.33	2.272
117WIRE	1200	.4924	15	10.4445	10.23	2.16
WIRE	60	.3315	15	6.02	6.61	-.587
WIRE	60	.3279	15	6.42	6.93	-.505
WIRE	60	.3272	15	9.144	8.22	.924

6.3.1 Sample Loss Analysis

Figure 6.2 indicates that power loss increases with frequency, which is expected. For the cases involving resin samples the power loss flattened out for high frequencies. To better understand this, more data needs to be taken because currently for each sample there are only three data points. The wire and air losses should be close to zero, and this might explain why the loss values are negative. If the air loss curve was not calibrated because of inconsistencies within the magnetic field then the curve might be offset by -0.5 Watts. This offset of the power curve also explains why at 60 Hz the samples have negative power loss.

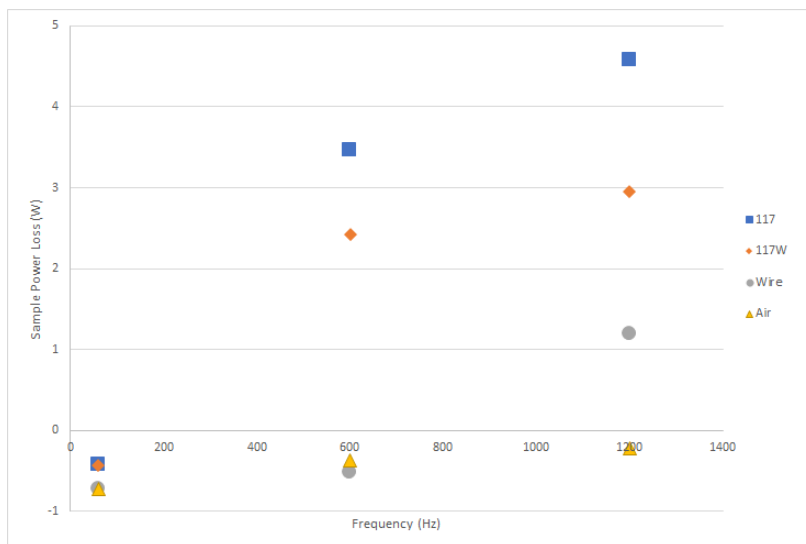


Figure 6.2: Power Loss vs. Frequency

Chapter 7

Error Discussion

This chapter will discuss all forms of error that possibly could have propagated through the experiment.

7.1 Sample Creation

In the sample creation there is error pertaining to the wire placement within the sample. In the sample creation measures were taken to place the wires uniformly throughout the resin by placing weights on the wire during the curing process. To check if the wire was flattened into the sample a cross section was taken at multiple points to check for uniformity of the wire. Though this was done at certain points the assumption was made that the portion of wire covered by resin would follow the pattern of the cross sections.

7.2 Magnetic Field Simulation

As discussed in Chapter 3, a model was created to compare with the experimental magnetic field data. The analysis went into detail how the experimental data was off from the theoretical data. The assumption is that the magnetic field in the leg is the same as the magnetic field in the centerpiece. The best way to solve for this magnetic field is to have a pickup coil around the centerpiece in the next round of testing.

7.3 Air Loss Equation and Experimental Data

Equation 6.4 was based on a combination of the Steinmetz model with Litz wire losses derived from a physical understanding of the system. Then data was taken to match the equation and solve for the coefficients to match the air loss equation. However, there could be other forms of loss not taken into account. One example is the testbench and the imprecision associated with it. The testbench was not exact because the AC source would oscillate .04 Amps from the designated current. The lugnut connection was not secure at first and had to be replaced because it melted the plastic container holding it. Another form of error was the HVAC system within the room. The air conditioning could not be controlled but was monitored using the thermocouples. The room would try to stay constant but there was approximately 2° of temperature change in the room. This room temperature error propagates into the data. This is because when the experiment would reach saturation with the environment it would need to change constantly to reach the environmental saturation temperature. The equation for calibration tried to account for this but the error needs to be noted. Lastly, during the sample taking process our procedure was to run the experiment for four hours per sample. However, one of our samples was taken at three hours and two samples were taken at three and a half hours. The samples had reached saturation and that is why the test was cut short.

Chapter 8

Conclusion

The motivation of this thesis was to better understand the losses within iron resin in order to predict the losses within high-speed electric motors. In order to solve this problem a calorimetric experiment was tested to relate an environmental saturation temperature with a power loss in the system. Then a series of tests were run to create an equation that could model losses within the ecore and the induction coils wire. Then experiments were run on samples of the 117 resin and 117 resin-wire. The observed losses compared against the expected air core losses permitted for the calculation of the sample losses. Figure 6.2 shows an increase in frequency is directly correlated to a power loss.

8.1 Future Work

The results of this experiment require further study. This experiment tested only the low-frequency high-voltage case. To come to a conclusion for high speed electric motor losses using an iron resin, a high-voltage and high-frequency data set is required because high-speed electric motors run at high-frequencies and high-voltages. To solve this problem a stronger AC source is essential because it can run a higher frequency and higher current through the test setup. Also to remove error from the system, in the calibration step having a pickup coil present throughout the entire experiment would be useful because the magnetic field could be monitored during the entire testing process. In addition, in the next round of experiments, the addition of an adjustable airgap to adjust the B field in our ecore would be advantageous. To adjust the B field a pulley string attached to the ecore could be implemented. This pulley system would allow for more versatility in the B field because the air gap could be changed incrementally at very small amounts. Lastly, finding an ecore composite that can handle

more than .5 Tesla as well as can operate correctly at higher temperatures is crucial to the next round of experiments. This experiment was limited because the ecore saturated at .5 Tesla. In order to properly characterize this iron resin for the Nasa Fixed Wing motor application a 1 Tesla E core is the minimum saturation value this experiment will need. Also if the core is being run at this higher current to create a higher B field the temperature the ecore is rated for will need to be increased.

8.1.1 Steinmetz Equation

This entire experiment was to approximate the Steinmetz coefficients of this iron resin. The Steinmetz equation gives values for the eddy and hysteresis losses which is important in characterizing the iron resin for use in high speed electric motors. To solve for this value at least three different magnetic field values are needed for Steinmetz equation to be calculated in SPEED. SPEED is a software application to model electric motor properties. The 117 Wire resin Steinmetz equation compared with 117 resin Steinmetz equation could give a relation between the fill factor and losses. The losses would be eddy and hysteresis losses which is important for the use of iron resin in high speed electric motors.

Chapter 9

References

- [1] L. Brocal, “Analysis and optimization of high-speed electric motor using iron-filled epoxy resin,” M.S. thesis, Universidad Pontificia Comillas.
- [2] J. Martin, “Development of high frequency airgap windings for high-power density electrical machines,” M.S. thesis, University of Illinois at Urbana Champaign, 2016.
- [3] A. Yoon, X. Yi, J. Martin, Y. Chen, and K. Haran, “A high-speed, high-frequency, air-core pm machine for aircraft application,” *IEEE Power and Energy Conference at Illinois (PECI)*, 2016.
- [4] K. S. Haran, D. Loder, T. O. Deppen, and L. Zheng, “Actively shielded high-field air-core superconducting machines,” *IEEE Transactions on Applied Superconductivity*, vol. 26, no. 2, pp. 98–105, March 2016.
- [5] P. Parthasaradhy and S. Ranganayakula, “Hysteresis and eddy current losses of magnetic material by epstein frame method-novel approach,” *The International Journal of Engineering And Science (IJES)*, pp. 85–93, 2014.
- [6] Sodano, Bae, Inman, and Belvin, “Concept and model of eddy current damper for vibration suppression of a beam,” *Journal of Sound and Vibration*, 2005.
- [7] Chetvorno, “Eddy current due to magnet,” Wikipedia, 2016.

Appendix A

Appendix

A.1 Matlab Code

A.1.1 Resin Project WNK

```
%Project Resin by Billy Kamerow
```

```
%Constants
```

```
u_0 = 4*pi*10^-7; %Permeability of vaccum—Air (henry/meter)
u_r = 3000;       %magnetic permeability of material 3C95 Ecore
u_m = 3;         %Permeability of Resin
u_s = 1.7921;
```

```
%Permeability of Resin Wire Combo calculated in Reverse_B_field.m
```

```
f_max = 1200; %High Frequency
f_mid = 600;  %Mid Frequency
f_min = 60;   %Low Frequency
```

```
B_max = .6737; %B fields
B_mid = .4102;
B_min = .2318;
```

```
l_1 = .0381254; % (m)—check lab manual Figure 1
l_2 = .030226;  % (m)—check lab manual Figure 1
```



```

l_3 = .0673354;      %(m)--check lab manual Figure 1
l_4 = .020447;      %(m)--check lab manual Figure 1
A_c2 = .00019523;   %(m^2) Cross Sectional Area of E core
A_gap = .00039857726; %(m^2) Cross Sectional Area of AIRGAP\
%B_max = .4          ;%400mT = .4T Magnetic Field of Saturation for

```

```

%Variables

```

```

lgap = [0];          %length of gap (m)
N     = 50;          %Turns of Transformer

```

```

%Reluctance Calculation

```

```

R_airgap= lgap/(u_0*A_gap);
R_resin= lgap/(u_0*u_m*A_gap);
R_sample= lgap/(u_0*u_s*A_gap);

```

```

R_c1= l_1/(u_0*u_r*A_gap);
R_c2= l_2/(u_0*u_r*A_c2);
R_c3= l_3/(u_0*u_r*A_c2);
R_c4= l_4/(u_0*u_r*A_c2);

```

```

R_Total_air=R_airgap + (2*R_c1) +(R_c2+ R_c3 + R_c4)/2;

```

```

% Assuming Air Gap is Air

```

```

R_Total_resin=R_resin + (2*R_c1) +(R_c2+ R_c3 + R_c4)/2;

```

```

% Assuming Air Gap is filled with Resin

```

```

R_Total_sample=R_sample + (2*R_c1) +(R_c2+ R_c3 + R_c4)/2;

```

```

% Assuming Air Gap is filled with Resin

```

```

%Flux Calculation

```

```

flux_max = B_max*A_gap;

```

```

% Using Ac2 because this is the max flux able to flow
through the smallest cross sectional area of the core

```

flux_mid = B_mid*A_gap;

flux_min = B_min*A_gap;

%Max Current Calculation

%Air

I_max_air = (flux_max*R_Total_air)/N;

I_max_resin = (flux_max*R_Total_resin)/N;

I_max_sample=(flux_max*R_Total_sample)/N;

I_mid_air = (flux_mid*R_Total_air)/N;

I_mid_resin = (flux_mid*R_Total_resin)/N;

I_mid_sample=(flux_mid*R_Total_sample)/N;

I_min_air = (flux_min*R_Total_air)/N;

I_min_resin = (flux_min*R_Total_resin)/N;

I_min_sample=(flux_min*R_Total_sample)/N;

%Max Inductance Calculation

%Air

L_air = (N^2)*(R_Total_air.^-1);

L_resin = (N^2)*(R_Total_resin.^-1);

L_sample = (N^2)*(R_Total_sample.^-1);

%MAX Voltage Calculation

V_I_max_air_fmax = L_air.*I_max_air*4*f_max;

V_I_max_resin_fmax = L_resin.*I_max_resin*4*f_max;

V_I_max_sample_fmax = L_sample.*I_max_sample*4*f_max;

V_I_mid_air_fmax = L_air.*I_mid_air*4*f_max;

V_I_mid_resin_fmax = L_resin.*I_mid_resin*4*f_max;

V_I_mid_sample_fmax = L_sample.*I_mid_sample*4*f_max;

$V_{I_min_air_fmax} = L_{air} * I_{min_air} * 4 * f_{max};$
 $V_{I_min_resin_fmax} = L_{resin} * I_{min_resin} * 4 * f_{max};$
 $V_{I_min_sample_fmax} = L_{sample} * I_{min_sample} * 4 * f_{max};$

$V_{I_max_air_fmid} = L_{air} * I_{max_air} * 4 * f_{mid};$
 $V_{I_max_resin_fmid} = L_{resin} * I_{max_resin} * 4 * f_{mid};$
 $V_{I_max_sample_fmid} = L_{sample} * I_{max_sample} * 4 * f_{mid};$

$V_{I_mid_air_fmid} = L_{air} * I_{mid_air} * 4 * f_{mid};$
 $V_{I_mid_resin_fmid} = L_{resin} * I_{mid_resin} * 4 * f_{mid};$
 $V_{I_mid_sample_fmid} = L_{sample} * I_{mid_sample} * 4 * f_{mid};$

$V_{I_min_air_fmid} = L_{air} * I_{min_air} * 4 * f_{mid};$
 $V_{I_min_resin_fmid} = L_{resin} * I_{min_resin} * 4 * f_{mid};$
 $V_{I_min_sample_fmid} = L_{sample} * I_{min_sample} * 4 * f_{mid};$

$V_{I_max_air_fmin} = L_{air} * I_{max_air} * 4 * f_{min};$
 $V_{I_max_resin_fmin} = L_{resin} * I_{max_resin} * 4 * f_{min};$
 $V_{I_max_sample_fmin} = L_{sample} * I_{max_sample} * 4 * f_{min};$

$V_{I_mid_air_fmin} = L_{air} * I_{mid_air} * 4 * f_{min};$
 $V_{I_mid_resin_fmin} = L_{resin} * I_{mid_resin} * 4 * f_{min};$
 $V_{I_mid_sample_fmin} = L_{sample} * I_{mid_sample} * 4 * f_{min};$

$V_{I_min_air_fmin} = L_{air} * I_{min_air} * 4 * f_{min};$
 $V_{I_min_resin_fmin} = L_{resin} * I_{min_resin} * 4 * f_{min};$
 $V_{I_min_sample_fmin} = L_{sample} * I_{min_sample} * 4 * f_{min};$

```

%%Power In Calculation
% P_air = V_air .* I_max_air;
% P_resin = V_resin .* I_max_resin;
%
%%Graph Plots
%
%%Lgap vs I (Current)
% figure;
% subplot(2,2,1)
% plot(lgap,I_max_air,lgap,I_max_resin)
% title('Current')
% legend('I max air','I max resin')
% xlabel('gap length (m)')
% ylabel('Current (Amps)')
%%Lgap vs Voltage
% subplot(2,2,2)
% plot(lgap,V_air,lgap,V_resin)
% title('Voltage')
% xlabel('gap length (m)')
% ylabel('Voltage (Volts)')
%%Lgap vs Power
% subplot(2,2,3)
% plot(lgap,P_air,lgap,P_resin)
% title('Power')
% xlabel('gap length (m)')
% ylabel('Power (Watts)')

```

A.1.2 *Experimental B*

```

%% Experimental B field Calculation
I=10;
N=16;

```

```

A = .00019523; %Cross section of small area
Vrms=[
.267;
2.58;
5.16;
]
f=[
60;
600;
1200;
];
w=2*pi*f;

```

```

%e=d(lambda)/dt
%integral of e then I get lambda

```

```

Bmag_small=(Vrms*sqrt(2))./(N*A*w);
%Bmag_big  =(Bmag_small*2);

```

```

%%

```

```

%Experimental B

```

```

I=15;

```

```

N=16;

```

```

A = .00019523; %Cross section of small area

```

```

Vrms=[
.405;
4.03;
8.07;
]

```

```

f=[
60;
600;
1200;
];
w=2*pi*f;

%e=d(lambda)/dt
%integral of e then I get lambda

Bmag_small=(Vrms*sqrt(2))./(N*A*w);
%Bmag_big  =(Bmag_small*2);
%%
%Experimental B'
I=10;
N=16;
A = .00019523; %Cross section of small area
Vrms=[
.178;
1.77;
3.5;
]
f=[
60;
600;
1200;
];
w=2*pi*f;

```

```

%e=d(lambda)/dt
%integral of e then I get lambda

Bmag_small=(Vrms*sqrt(2))./(N*A*w);
%Bmag_big  =(Bmag_small*2);

%%
%Experimental B'
I=15;
N=16;
A = .00019523; %Cross section of small area
Vrms=[
.268;
2.61;
5.24;
]
f=[
60;
600;
1200;
];
w=2*pi*f;

%e=d(lambda)/dt
%integral of e then I get lambda

Bmag_small=(Vrms*sqrt(2))./(N*A*w);
%Bmag_big  =(Bmag_small*2);
%%

```

```

%Experimental B for 117 15 A
I=15;
N=16;
A = .00019523; %Cross section of small area
Vrms=[
0.41;
4.09;
8.19;
]
f=[
60;
600;
1200;
];
w=2*pi*f;

%e=d(lambda)/dt
%integral of e then I get lambda

Bmag_small=(Vrms*sqrt(2))./(N*A*w);
%Bmag_big  =(Bmag_small*2);
%%
%Experimental B for 117WIRE 15 A
I=15;
N=16;
A = .00019523; %Cross section of small area
Vrms=[
0.414;
4.11;

```



```

8.2;
]
f=[
60;
600;
1200;
];
w=2*pi*f;

%e=d(lambda)/dt
%integral of e then I get lambda

Bmag_small=(Vrms*sqrt(2))./(N*A*w);
%Bmag_big  =(Bmag_small*2);
%%
%Experimental B for WIRE 15 A
I=15;
N=16;
A = .00019523; %Cross section of small area
Vrms=[
0.276;
2.73;
5.45;
]
f=[
60;
600;
1200;
];

```

$$w=2*\pi*f;$$

$$\%e=d(\text{lambd})/dt$$

$\%$ integral of e then I get lambda

$$\text{Bmag_small}=(V_{\text{rms}}*\text{sqrt}(2))./(N*A*w);$$

$$\%B_{\text{mag_big}}=(\text{Bmag_small}*2);$$

A.2 Samples

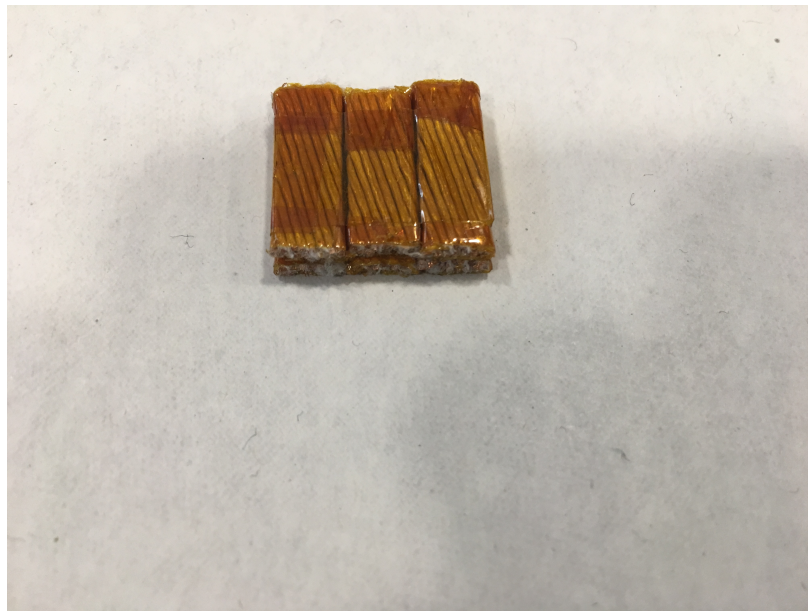


Figure A.1: Wire Sample

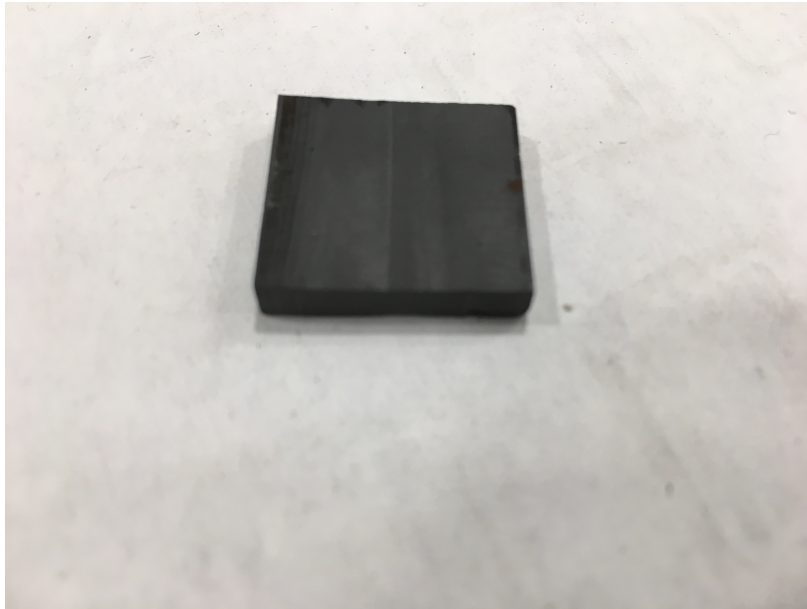


Figure A.2: Resin Sample

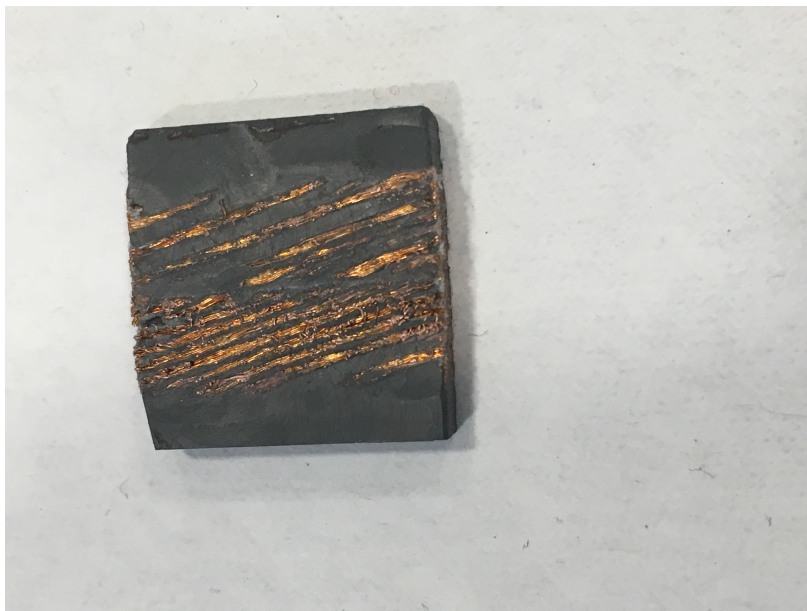


Figure A.3: Wire Resin Sample